ADVANCED QUANTUM TECHNOLOGIES
www.advquantumtech.com

Exploring Conductance Quantization Effects in Electroformed Filaments for Their Potential Application to a Resistance Standard

Jordi Suñé, Fernando Aguirre, Mireia Bargalló González, Francesca Campabadal, and Enrique Miranda*

The ballistic conduction through narrow constrictions connecting charge reservoirs exhibits conductance quantization effects. Since the quantum of conductance $G_0 = 2e^2/h$ is only related to fundamental constants of nature, these effects might allow the implementation of a standard of resistance, fulfilling the requirements of the 2019 revised International System of Units. Moreover, this standard would be able to work at room temperature and without a magnetic field, thus allowing its on-chip implementation. In this work, the authors propose that breakdown filaments in thin oxide layers might be useful to this purpose. In particular, conductance quantization effects in nanolaminate Al_2O_3/HfO_2 dielectrics are reported and the role of intrinsic values of conductance and extrinsic parasitic elements are analyzed. The fact that breakdown filaments are irreversible is an advantage due to their expected stability and to the lack of cycle-to-cycle variations (as compared to resistive switching devices). Although the reported sample-to-sample variations are still too large for a real application, there is room for improving the controlover breakdown filaments through material design and electroforming conditions. Provided that this control is achieved, an on-chip implementation of a resistance standard for the realization of self-calibrating electrical systems and equipment with zero-chain traceability would be possible.

1. Introduction

According to the Landauer approach to electron transport, the ballistic conduction through narrow constrictions connecting two external charge reservoirs, exhibits conductance quantization effects.[1] This configuration is often referred to as a quantum point contact (QPC). Conductance quantization comes from the fact that the width of the constriction is comparable to the wavelength of the electrons so that there is energy quantization in the direction transversal to the electron transport. If the constriction is very narrow, only a small number of the quasi-1D modes (or channels) contribute to the conduction. This number is roughly determined by the ratio of the constriction width to the electron wavelength, and the conductance is given by

$$G = \frac{2e^2}{h} \sum_{1}^{N} \tau_n \tag{1}$$

where N is the number of channels and τ_n their individual transmission coefficients, which are related to backscattering. In the limit of transmission coefficient equal to 1 for all the transport modes, $G = NG_0$, where $G_0 = 2e^2/h$ is the quantum of conductance which only depends on fundamental constants, e being the electron charge and h the Planck constant. The number 2 arises from assuming spin degeneracy. Assuming that there is no energy quantization in the reservoirs, a redistribution of the current among the current-carrying modes at the reservoir/conductor interfaces must occur. This naturally results in the existence of a contact resistance related to an energy funneling effect, though the ballistic conductor itself has zero resistance.[2]

Conductance quantization was first experimentally demonstrated by modulating the width of a 2D electron gas in a semiconductor with a split-gate structure close to the absolute zero of temperature. In these experiments, conductance appeared to be quantized in integer multiples of G_0, as predicted by theory.[3,4] The Fermi wavelength in a semiconductor is rather large since the occupied/unoccupied states are very close to the minimum/maximum of the conduction/valence band. On the contrary, the Fermi wavelength in a metal is of the same order of

J. Suñé, F. Aguirre, E. Miranda
Departament d'Enginyeria Electrònica
Universitat Autònoma de Barcelona (UAB)
Campus de Bellaterra, Edifici Q, 08193, Cerdanyola del Vallès, Beallaterra 08193, Spain
E-mail: jordi.sune@uab.cat

M. Bargalló González, F. Campabadal
Institut de Microelectrònica de Barcelona (IMB-CNM-CSIC)
Spain, Campus UAB, Cerdanyola del Vallès 08193, Spain

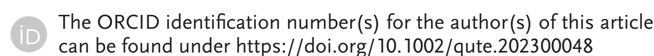
The ORCID identification number(s) for the author(s) of this article can be found under https://doi.org/10.1002/qute.202300048

© 2023 The Authors. Advanced Quantum Technologies published by Wiley-VCH GmbH. This is an open access article under the terms of the Creative Commons Attribution License, which permits use, distribution and reproduction in any medium, provided the original work is properly cited.

DOI: 10.1002/qute.202300048

magnitude as the atomic separation (about 0.5 nm) so that conductance quantization only occurs in a filament of atomic dimensions. In addition, since the confining potential well is much narrower in filamentary QPCs, the transverse energy level spacing is considerably larger than in semiconductors so that conductance quantization can be observed even at room temperature. On the contrary, conductance quantization in semiconductors can only be observed at cryogenic temperatures. Several techniques have been used to reveal conductance quantization in metallic QPCs including mechanically controllable break-junctions and scanning tunneling microscope (STM) retraction experiments.[5,6] Furthermore, combining STM with high-resolution transmission electron microscopy, has allowed relating the electrical results to the atomic configuration of the filament. In particular, it was shown that one chain of single Cu atoms contributed with G_0 to the measured conductance and two parallel chains with $2G_0$.[7] This is a very relevant observation because in the case of filamentary QPCs there is always the uncertainty of whether discrete conductance jumps are strictly due to conductance quantization or to geometrical changes in the atomic structure of the filament. Also worth mentioning is the use of electrochemical etching/deposition methods which have shown enough control over the size of a metal wire to achieve predetermined levels of quantized conductance.[8]

Interestingly, in recent years, conductance quantization effects have also been reported in conducting filaments (CFs) created during the breakdown (BD) of thin gate oxides in metal-oxide–semiconductor (MOS) devices [9] as well as in resistive switching (RS) devices.[10–16] In both cases, the devices are simple capacitor structures with an oxide and two metal (or semiconductor) electrodes which are electrically stressed to form a conducting filament of atomic-size dimensions. Depending on whether one of the electrodes is an electrochemically active metal (Cu or Ag, for example) the filament is formed by metal atoms or oxygen vacancies.[10,17] The main difference between BD and RS filaments is that the former are irreversible whereas the latter can be partially dissolved and reconstructed by the application of electric fields of (usually) opposite polarity. In this work, we deal with conductance quantization effects in BD filaments, a subject that has received very little attention in the literature.[9,18,19]

As stated above, in the type of devices we consider in this work, the conductance jumps correspond to structural modifications of the filamentary pathway caused by ion motion which subsequently affects electron injection. These are electro-ionic effects which cause the conductance to show hysteretic effects. In fact, when the voltage is increased, the atomic structure of the CF is modified and, when voltage is reduced back to zero, the device shows a different $I(V)$ characteristic. For this reason, observation of quantum steps in the conduction characteristics of RS or BD filaments should be more appropriately considered to be in the quantum regime rather than in the quantized regime.[20] However, the fact is that filaments with a width of few atoms also show a conductance quantized in multiples of G_0.

Memristive devices promise applications such as high-density multi-state resistive random access memories and the implementation of almost analog weights (synapses) in neuromorphic neural networks. Moreover, since the quantum of conductance $G_0 = 2e^2/h$ is only related to physical constants that are assumed to have a fixed value in the revised international system of units (SI), conductance quantization in atomic-scale CFs might be exploited for the realization of a quantum-based resistance standard.[21] It is likely that this realization would not achieve the accuracy of the conventional resistance standard which is based on the quantum-Hall–effect. However, it has other advantages such as its capability of operating at room temperature, harsh environments, and without the application of a magnetic field. Due to these properties and the compatibility with CMOS technology, these QPC devices might allow the on-chip implementation of a resistance standard required for the realization of self-calibrating electrical systems and equipment with zero-chain traceability . In this work, we explore QPC effects in irreversible BD filaments and analyze their electrical properties with an eye toward the implementation of this kind of standard. In particular, we consider MOS structures with three different dielectric layers: HfO_2, Al_2O_3, and a nanolaminate insulator which combines ultrathin layers of these two oxides.

In the past decade, different ultrathin insulator layers have been explored to replace SiO_2 gate oxides in order to cotinue downscaling CMOS devices. Nanolaminates of these oxides have also been considered and, in particular, HfO_2/Al_2O_3 structures have attracted great interest because of their excellent characteristics such as chemical and thermal stability, high BD field, low leakage, and high dielectric constant.[22–25] Al_2O_3 has a large band gap of ≈8.8 eV, not very large relative permittivity ($\kappa \approx 9$), high BD field and it is known to be a good barrier to ionic transport. On the other hand, HfO_2 has a rather a high relative permittivity ($\kappa \approx 20 - 25$) but higher leakage (bandgap ≈5.5 eV) and significantly lower BD voltage. It has been demonstrated that nanolaminates of these materials have intermediate values of the dielectric constant, leakage current, and BD strength, thus allowing to tune the properties of the stacked insulator to what is required for different applications.[22,26] Since we are interested in increasing the control of the CF formation to ensure that it has stable QPC properties, and knowing that the oxygen diffusion (and drift) controls the dynamics of CF formation, two key figures of merit are the oxygen diffusion frequency prefactor, D_O, and the thermal activation energy, E_a. Although many different values have been reported in the literature depending on the microstructure of the oxide (crystalline, amorphous, bulk, thin-layer,...), typical values for Al_2O_3 are $D_\mathrm{O} \approx 10^{-14}$ cm^2 s^{-1} and $E_\mathrm{a} \approx 1.3$ eV,[27] and for HfO_2, $D_\mathrm{O} \approx 10^{-8}$–$10^{-4}$ cm^2 s^{-1} and $E_\mathrm{a} \approx 0.52$ eV.[28] Since D_0 is much smaller and E_a is significantly larger in Al_2O_3, its oxygen diffusion coefficient, given by $D = D_0 \exp(-E_\mathrm{a}/K_\mathrm{B}T)$, is expected to be several orders of magnitude smaller than that corresponding to HfO_2. In fact, alumina is well-known to have a very low oxygen self-diffusion coefficient and has been used as an efficient oxygen barrier in the microelectronics industry. Thus, Al_2O_3 layers are expected to act as oxygen diffusion barriers in any Al_2O_3/HfO_2 stack combination as those considered in this work.

Engineering the oxide layer requires a deep understanding of the kinetics of nanoionic effects for a proper selection of the involved materials. Unfortunately, proper design rules relating material properties and operation conditions to the observation of quantized conductance effects are still missing. However, there have been attempts to control the shape of the CFs and QPC conductance levels by modifying the material structure, device design, processing conditions, electroforming process, and

© 2023 The Authors. Advanced Quantum Technologies published by Wiley-VCH GmbH

25119044, 2023, 7, Downloaded from https://onlinelibrary.wiley.com/doi/10.1002/qute.202300048 by Readcube (Labtiva Inc.), Wiley Online Library on [03/10/2023]. See the Terms and Conditions (https://onlinelibrary.wiley.com/terms-and-conditions) on Wiley Online Library for rules of use; OA articles are governed by the applicable Creative Commons License

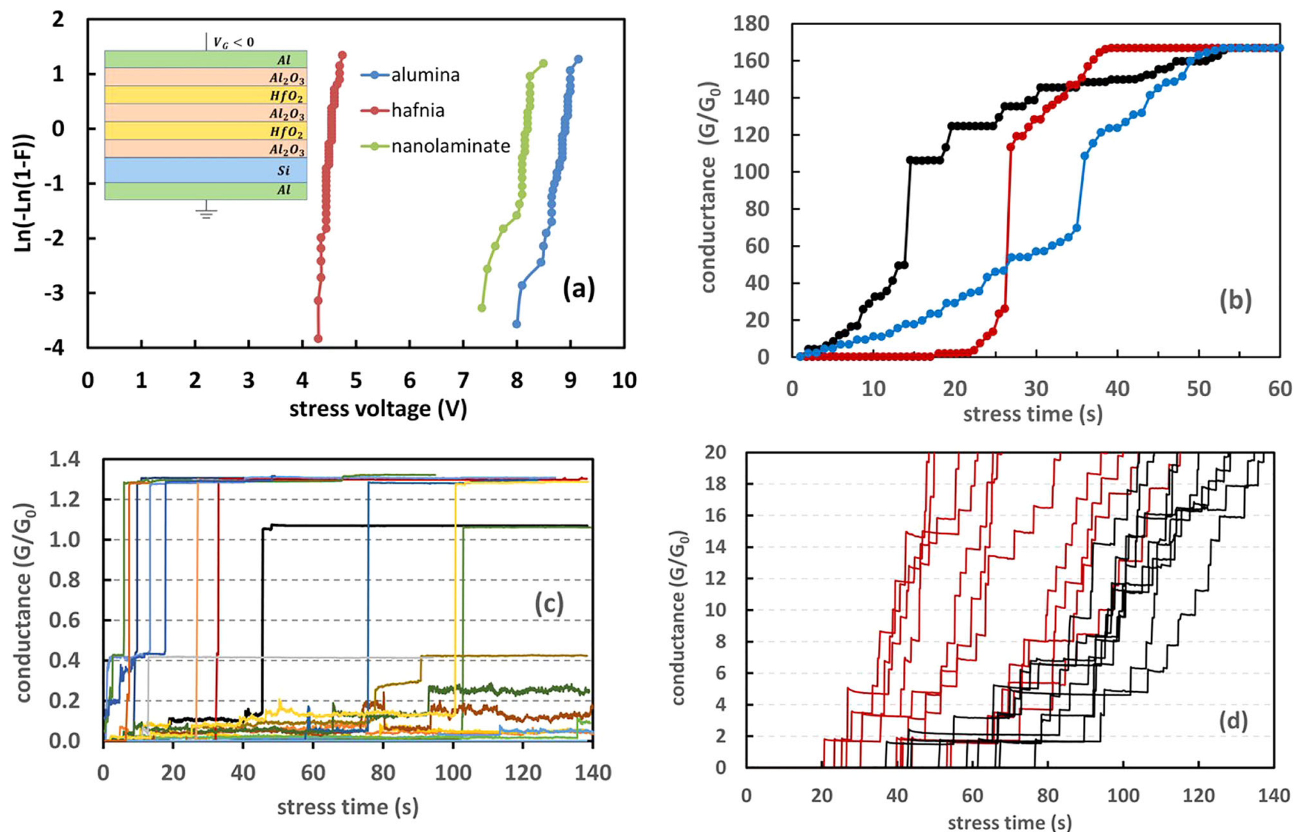

Figure 1. Breakdown characteristics of single-layer and nanolaminate dielectrics. a) Cumulative breakdown distributions in the Weibull plot. The results correspond RVS with ramp rate of 0.27 V s^{-1}. b) Evolution of conductance during CVS at −7.7 V of three samples with Al_2O_3 dielectric. c) Evolution of conductance during CVS at −4 V of several samples of HfO_2. d) Evolution of conductance in several HfO_2/Al_2O_3 nanolaminate samples stressed under CVS conditions at −6,8 (black curves) and −7 V (red curves).

electrical stress methods. For example, Aga et al. introduced a Ti barrier layer in their Cu/Ti/HfO_2/TiN structures and reduced the stress voltage ramp rate to control the Cu^+ reaction/diffusion processes involved in the SET/RESET transitions.[29] Moreover, with a forming process at high temperature they were able to control up to 64 levels (6 bits) of G_0.[30] Mahata et al. incorporated a layer of Pt nano particles in the middle of a $HfAlO_x$ film and claimed an enhanced control of the QPC filament due to the increased electrical field in the middle of the dielectric.[31] Xue justified the control of conductance during the RESET process because of the negative current feedback and used an ITO electrode to control diffusion and reaction dynamics of oxygen vacancies.[32] Bilayer dielectrics and metal barrier layers have also been used to improve the device design in the QPC limit. In particular, Lim et al. demonstrated improved control of QPC conductance levels in an ECM cell by moving from Cu/Cu_2S/W to Cu/HfO_2/Cu_2S/W (oxide bilayer) and to Cu/HfO_2/Ta/Cu_2S/W (barrier layer plus oxide bilayer).[33] Following a similar strategy we will consider HfO_2/Al_2O_3 nanolaminate structures to control the electrical properties of QPC in BD filaments.

2. Results

In this paper, we study the breakdown properties of HfO_2, Al_2O_3, and $Al_2O_3/HfO_2/Al_2O_3/HfO_2/Al_2O_3$ nanolaminate insulators (inset of **Figure 1**a) fabricated on a silicon wafer and with Al top/bottom electrodes (Experimental Section). The thickness of the dielectric is ≈ 10 nm in the three cases. In previous works, a complete electrical characterization of these insulator stacks was performed, including the measurement and analysis of the current–voltage, $I(V)$, and the capacitance–voltage, $C(V)$, characteristics.[26,34]

In this work we are mainly concerned with the BD of the layers and we have performed both ramped voltage stresses (RVS) and constant voltage stresses (CVS). The cumulative BD distributions, $F(V)$, obtained under a RVS with ramp rate of 0.27 V s^{-1} are compared in the Weibull plot, that is, by representing $\mathrm{Ln}(-\mathrm{Ln}(1-F))$ versus V (Figure 1a). Notice that the nanolaminate dielectric strength is, as expected, higher than that of HfO_2 and smaller than (but closer to) that of Al_2O_3. The results of HfO_2 and Al_2O_3 were fitted to the usual Weibull distribution while the statistical distribution of the nanolaminate is nicely reproduced by combining the distributions of the two single oxide layers according to an analytical model for defect percolation of multiple-layer gate stacks.[35,36]

It is well-known that slow ramp rates allow a better control of the size of CFs and the observation of QPC effects. Hence, CVS is expected to allow even a better control and we have focused on this type of stress. Lower stress voltages are expected to favor narrow filaments and the formation of QPCs. However, voltage

© 2023 The Authors. Advanced Quantum Technologies published by Wiley-VCH GmbH

25119044, 2023, 7, Downloaded from https://onlinelibrary.wiley.com/doi/10.1002/qute.202300048 by Readcube (Labtiva Inc.), Wiley Online Library on [03/10/2023]. See the Terms and Conditions (https://onlinelibrary.wiley.com/terms-and-conditions) on Wiley Online Library for rules of use; OA articles are governed by the applicable Creative Commons License

cannot be too low because the time to BD increases exponentially when the voltage is reduced. Thus, the stress voltage for each type of dielectric was chosen according to their dielectric strength, as determined by the RVS experiments. The evolution of the normalized conductance (G/G_0) during these CVS experiments are shown in Figure 1 for the three types of insulators. Conductance at each $I(V)$ measurement point was calculated by dividing the measured current by the stress voltage. The post breakdown $I(V)$ is essentially linear so that the conductance is roughly independent of voltage.

The single-layer Al_2O_3 insulator was stressed under $V_G = -7.7$ V. The evolution of conductance shows some large discrete jumps which correspond to changes of up to $\approx 50\ G_0$ and also significant continuous evolutions of G between these jumps (Figure 1b). Thus, in this insulator, the BD events are rather uncontrollable and no clear QPC effects are observed. In HfO_2-based devices stressed under $V_G = -4$ V, the signature of preferred atomic-sized constrictions with conductance of the order of G_0 is found (Figure 1c). A significant number of devices reach a conductance level $G = 1.3\ G_0 \pm 0.02\ G_0$, which is rather stable and shows small variations from sample to sample (about $\pm 1.5\%$). However, not all the devices reach this level, and many intermediate conductance jumps in the sub-G_0 regime are often found. Thus, because of large device-to-device variations, these devices are not useful for a resistance standard application. Finally, the structures with a nanolaminate dielectric have been stressed under four different gate voltages (-6.5; −6.8; −7.0, −7.2, and −7.4 V). In this case, the evolution of the current shows a series of very repeatable conductance levels of the order (though smaller) of $2G_0$ in all the devices (Figure 1d). This is a clear signature of QPC behavior. These results suggest that the shape of the CFs is modified in the nanolaminate dielectric and that it allows a much better control of its constriction size.

It has been well established that when a MOS structure is subjected to electrical stress, defects (traps) are generated in the oxide. These defects can be oxygen vacancies which drift from the cathode electrode under the action of the electric field, and which pile up to form conductive regions within the insulator. When a path of vacancies percolates and connects both electrodes, a BD filament is created. This is the assumption of the percolation model, which is by far the most widely accepted picture for the BD statistics.[37,38] If the most constrictive part of the formed CF has atomic-size dimensions, then it behaves as a QPC.[9,18,19]

In this paper, we mainly focus on the distribution of conductance levels after the BD jumps, while the distribution of the time to successive BD events was carefully examined in previous works.[39,40] In these previous analysis, it was demonstrated that the time-dependent clustering model (TDCM) is needed to explain the deviations from the Weibull model in the high percentile region of the first BD distribution.[41] Moreover, this was shown to be due to variability in the background current of the devices (probably related to insulator thickness variations). It was also demonstrated that the successive BD distributions could be nicely fitted with the TDCM up to approximately the tenth event.[39] The disagreement between model and experiment for larger number of events was attributed to time correlations which can be positive or negative.[42–44] The absence of correlation means that the rate of BD path generation during stress does not depend on the BD time and/or spatial location of previously opened BD filaments. However, it is difficult to exclude these effects when multiple events occur in a single device and when one of the electrodes is a semiconductor. In particular, a negative correlation is expected to occur if the current associated with each BD filament is large enough to reduce the oxide voltage due to series resistance effects. On the other hand, reasons for positive correlations also exist, such as the propagation of the BD filament to nearby regions, as it has been experimentally observed,[45] due to the local modification of the oxide microstructure in the surroundings of the CF.[46] The reduction of the insulator electric field due to the voltage drop in the series resistance reduces the rate of generation of new CFs and, hence, the time to successive BD events. This causes a negative time correlation which was introduced into the TDCM using the E-model of BD acceleration.[47] The joint consideration of clustering and correlation effects allowed to nicely model the successive BD statistics up to the 20th event and beyond.[40] Full understanding of the successive time to BD statistics confirms that we are dealing with the generation of CFs in different locations of each sample, that is, different defect percolation paths (filaments). Moreover, the appearance of negative correlations suggests the importance of considering parasitic elements such as the series resistance.

Let us now focus on the analysis of the conductance jumps and levels reported in Al_2O_3/HfO_2 nanolaminates (Figure 1d). We will analyze the results (**Figure 2**a) which correspond to a CVS experiment performed at −7 V on 40 samples.

Direct inspection of the data shown in Figure 2a reveals that there is a series of levels with conductance values at integer multiples of $\approx 2G_0$ (actually slightly below smaller than this value, as we will discuss below). Several physics-based explanations for the actual value of G will be given but, in any case, these results strongly suggest conductance quantization or, at least, conduction through filaments of atomic-size dimensions showing quantum effects. If we consider the statistics of all the conductance readings in a single sample, we find a distribution of conductance peaks as shown in Figure 2b. The peaks are narrower than $0.05\ G_0$, almost equally spaced (at least the first 4–5 peaks, as shown in the inset) and with a separation of $\approx 1.7\ G_0$. About 60 conductance levels are reported, which correspond to the successive formation of an equivalent number of filaments. Notice that the height of the peaks does not correspond to the prevalence of the different conductance levels or to their intrinsic stability. On the contrary, they are related to the number of measurements between successive BD events because each level is interrupted by the occurrence of a new BD event. If we consider the whole ensemble of measurements (all measured conductance points in 40 samples), the histogram of conductance is the one shown in Figure 2c. Although rather large sample-to-sample variations are observed, the first four peaks do not overlap with each other and are clearly distinguishable. The mean of the first conductance level (see the inset of Figure 2c) is $1.67\ G_0$ and its standard deviation $\approx 0.1\ G_0$. Higher levels show a larger dispersion of results (higher standard deviation). This is because the conductance of the nth level is the sum of conductance of n filaments in parallel and this increases the variance since $\sigma_G^2(n) = \sum_1^n \sigma_{Gi}^2$ with $\sigma_G(n)$ and σ_{Gi} being the standard deviations of the total conductance for n filaments and that of each individual filament. Again, the height of the peaks is only related to the time elapsed

© 2023 The Authors. Advanced Quantum Technologies published by Wiley-VCH GmbH

25119044, 2023, 7, Downloaded from https://onlinelibrary.wiley.com/doi/10.1002/qute.202300048 by Readcube (Labtiva Inc.), Wiley Online Library on [03/10/2023]. See the Terms and Conditions (https://onlinelibrary.wiley.com/terms-and-conditions) on Wiley Online Library for rules of use; OA articles are governed by the applicable Creative Commons License

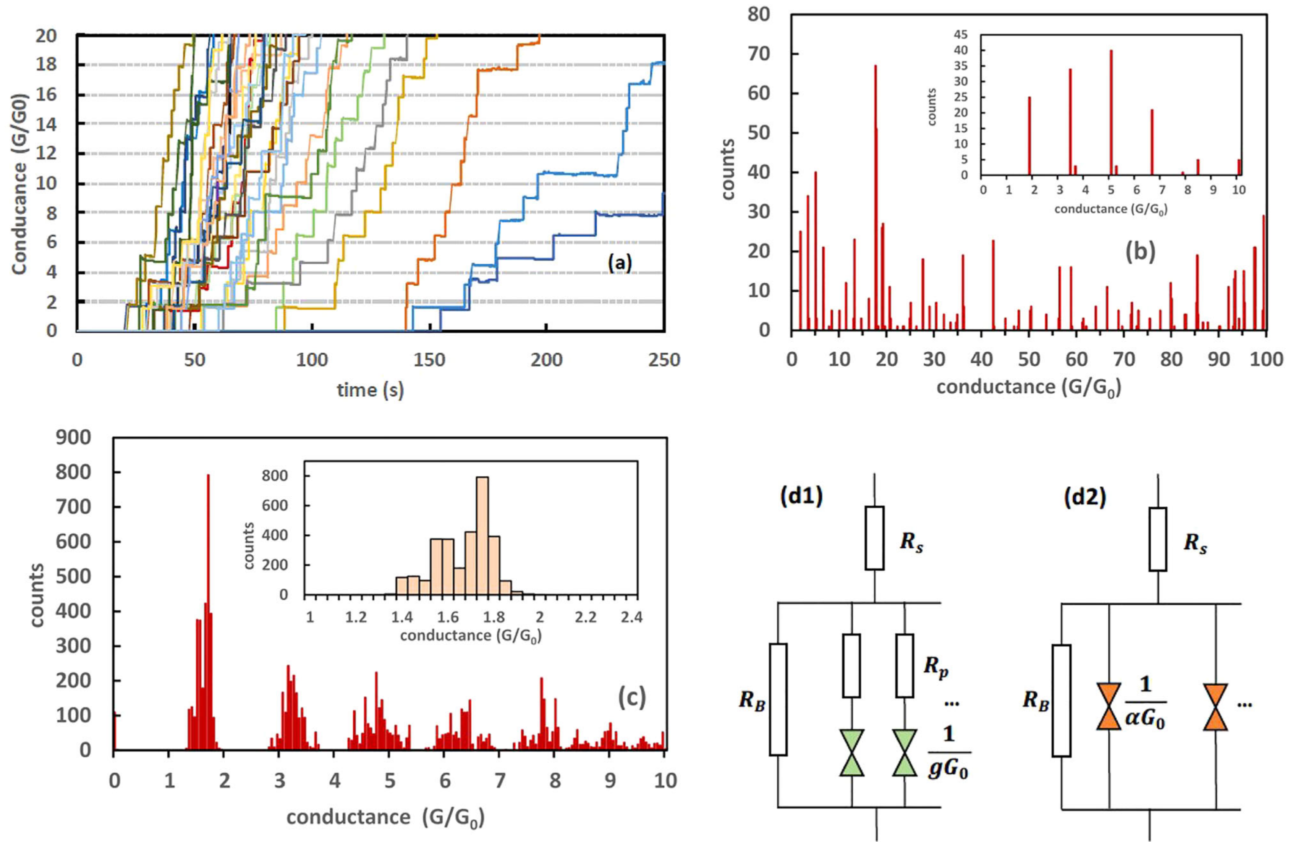

Figure 2. Data and analysis of conductance levels corresponding to multiple BD events in a HfO_2/Al_2O_3 nanolaminate dielectric. a) Raw data: evolution of conductance (normalized to G_0) during a CVS performed at −7 V on 40 samples; b) Histogram of conductance for a single sample considering all the current readings during the stress. Peaks reveal the quantized levels observed in (a). Inset shows the detail of the first peaks; c) Histogram of conductance (all readings) considering all the stressed samples. The inset shows the details of the first conductance level. The peak width is mainly due to device-to-device variations; d) Equivalent circuits used to analyze the data considering parasitic resistances, level degeneracy, and transmission coefficients, as defined in the text. The differences between both alternative circuits are discussed in the text as well.

between the successive BD events. Since this time decreases with the number of events, n, and $\sigma_G(n)$ increases, higher order peaks are less pronounced and tend to overlap.

To further analyze the obtained results and to consider the possible application of these QPCs for the realization of an on-chip resistance standard, we need to evaluate the parasitic elements which affect the measured conductance, G_{exp}.[21] First, it is evident that we cannot a priori ignore the existence of an external series resistance, R_S, which reduces G_{exp}. This resistance is in series with the overall parallel combination of QPC filaments and, in our case, it can be particularly significant because one of the electrodes is silicon (i.e., higher resistance than a metal). On the other hand, each QPC path might also be affected by a local parasitic series resistance, which has been often taken into account to describe the shift of the conductance peaks to lower values of conductance.[48] When we consider the shape of the filament that bridges the electrodes though the whole insulating layer (≈10 nm) we need to take into account that the actual constriction where conductance quantization takes place is a very short region of atomic-size dimensions (likely smaller than 1 nm) in which transport is essentially ballistic (only elastic scattering taking place). Transport in the rest of the filament is expected to be essentially diffusive and should be consider as a part of the external charge reservoirs in the Landauer–Datta approach. These access regions are still very narrow so that they certainly add a resistance in series with the filament. Note that this resistance is not the global series resistance of the device but must be considered as a separate parasitic element for each filament. Unfortunately, this parasitic resistance cannot be decoupled from the transmission coefficient of the quantum modes in the QPC.[48] Finally, a resistance parallel to all the QPC paths, R_B, must also be considered, which represents the leakage conduction through the bulk of the oxide without BD paths. Given these considerations, we can choose between two different though equivalent electrical circuits (Figure 2d).

These circuits represent two alternative descriptions of the non-ideality of the QPC paths. In circuit d1, all the parasitic effects within the QPC path are incorporated through the parasitic resistance, R_p. The transmission coefficient is supposed to be equal to one (purely ballistic transport), as suggested by Milano.[21] In both circuits, g represents the number of modes contributing to the conductance of the QPC. In our case, we have assumed $g = 2$ because a number of modes smaller than two cannot explain that the experimental conductance is larger than G_0. A detailed discussion about this issue will be presented after analyzing the experimental results. In circuit d2, no local

© 2023 The Authors. Advanced Quantum Technologies published by Wiley-VCH GmbH

25119044, 2023, 7, Downloaded from https://onlinelibrary.wiley.com/doi/10.1002/qute.202300048 by Readcube (Labtiva Inc.), Wiley Online Library on [03/10/2023]. See the Terms and Conditions (https://onlinelibrary.wiley.com/terms-and-conditions) on Wiley Online Library for rules of use; OA articles are governed by the applicable Creative Commons License

resistance is considered, and all the non-idealities are incorporated through the parameter $\alpha = gT$, where T is an equivalent transmission coefficient which represents both the actual transmission of the QPC channels and the effects of the local access resistance. Using a circuit combining both R_p and α (i.e., separating backscattering and series resistance effects) might seem more realistic. However, this only complicates the picture, and it is completely useless because, being these two elements in a serial configuration without an accessible internal node, these effects cannot be discriminated by electrical measurements. Our arbitrary choice is to use circuit d1, so that we will deal with the determination of three parameters, R_S, R_B, and α. In any case, once α is obtained, R_p, the parameter of the alternative circuit d1, can be directly calculated as $R_p = (g-\alpha)/(\alpha g G_0)$.

Let us now extract the parameters of circuit d2 from the experiments on Al_2O_3/HfO_2 nanolaminates reported in Figure 2. The bulk resistance R_B can be directly extracted from the initial current–voltage characteristic (i.e., before the first BD event). The pre-BD $I(V)$ curve is strongly non-linear but we have measured R_B at the stress voltage in order to be consistent with all the other resistances extracted for the CFs. The distribution of R_B obtained for the whole set of samples is shown in **Figure 3**a. The mean value of R_B is $\mu_B = 8.7 \times 10^6$ and the standard deviation $\sigma_B = 1.9 \times 10^6$. These values are significantly higher than the CF resistance, which is of the order of $(nG_0)^{-1} = (12.9/n)$ K. In the worst-case scenario, which corresponds to $n = 1$, the error introduced by R_B would be ≈1.5%. Although rather small, this uncertainty has to be taken into account when designing structures with the higher accuracy needed for a resistance standard.

Having determined R_B and its dispersion, let us now focus on the extraction of α and R_S. A first-order estimation of R_S can be obtained by the resistance measured at the end of the stress of each sample. In this limit, the conductance associated to all the conducting filaments is very large (typically ≈100 G_0) and the total resistance is expected to be mainly controlled by R_s. Thus, ignoring the resistance of the QPC filaments, we obtain an upper limit for R_s with mean $\mu_{Rs} = 123\ \Omega$ and standard deviation $\sigma_{Rs} = 29\ \Omega$.

A more realistic procedure is to use Equation (2) for the simultaneous extraction of R_s and α by fitting R_{exp} versus $1/n$ using the least-square method. Given that

$$R_{exp} = R_s + \frac{1}{n\alpha G_0} \tag{2}$$

we can extract α from the slope and R_s from the y-intercept. An example of the method is given in Figure 3b. In this way, α can be determined quite accurately. Nevertheless, the method is quite deficient for R_s (the y-intercept can even take negative values in some samples). To avoid this problem, we determine R_S by fitting the evolution of G_{exp} versus the number of events,once α has been determined. In the case of zero series resistance, the ideal evolution of conductance should be given by $G_{ideal} = n\alpha G_0$ and the magnitude of the conductance jumps would be independent of n, that is, $\Delta G_{ideal}\ (n \to n+1) = \alpha G_0$.On the other hand, if $R_s \neq 0$, the experimental conductance is given by

$$G_{exp} = \frac{n\alpha G_0}{1 + R_s n\alpha G_0} \tag{3}$$

and the expected experimental magnitude of the conductance jumps is

$$\Delta G_{exp}\ (n \to n+1) = \frac{\alpha G_0}{1 + R_s\alpha G_0\left(1 + 2n + n(n+1)R_s\alpha G_0\right)} \tag{4}$$

Keeping the value extracted for α, we fit G_{exp}versus n data to obtain a much more accurate value of R_s. In this way, the model nicely fits the experimental data (Figure 3c).

The distribution of α (Figure 3d) has a mean value $\mu_\alpha = 1.67$ and standard deviation $\sigma_\alpha = 0.13$. Considering $\pm\sigma_\alpha$ as the standard error, the accuracy related to sample-to-sample variations is ≈15%. Notice that the distribution of α and also the standard deviation are very similar to those obtained for the first conductance level, so that we can conclude that α determines the experimental conductance and its variations, at least for the first level. The distribution of the extracted series resistance is quite wide (Figure 3e). It has a mean value $\mu_{Rs} = 80\ \Omega$ and standard deviation $\sigma_{Rs} = 53$. Considering $\pm\sigma_{Rs}$ as the standard error, this means that the error of the extracted R_s is of the order of more than 100%. However, the inset of Figure 3c shows that the series resistance has a very limited impact on the value of the measured conductance for the very first levels. For the first level, $G_{ideal} = 1.67\ G_0$ and the experimental conductance calculated from Equation (3) is $G_{exp} = 1.65\ G_0$. Moreover, considering resistances corresponding to $\pm\sigma_{Rs}$ yields $1.64\ G_0 < G_{exp} < 1.66\ G_0$. This means that for the first level, the error in G_{exp} due to R_s is only ≈ 2%.

On the other hand, looking at the details of the first discrete G_{exp} levels (all the levels show a similar behavior), we realize that there is a conductance transient starting after each conductance jump (Figure 3f). This type of conductance transient has also been observed in the SET and RESET processes of RS devices.[49] During this transient, G_{exp} decreases with time toward saturation until it is suddenly interrupted by the occurrence of the subsequent BD event. The evolution of the experimental conductance is nicely modeled with two exponentials terms with different time scales.

$$G_{exp}\ (t) = G_{final} + \Delta G_1 \exp\left(-\frac{t}{\tau_1}\right) + \Delta G_2 \exp\left(-\frac{t}{\tau_2}\right) \tag{5}$$

The fastest evolution has a typical characteristic time $\tau_1 \approx 1$ s and the slowest one, $\tau_2 \approx 10$ s. We speculate that these might correspond to two processes involving discharging effects and the reconfiguration of the atomic structure of the QPC, respectively. The total change of conductance during the transient is ≈ 0.2 G_0 and it does not depend on its initial value, as revealed by the fact that there is an almost perfect correlation between the initial and final values of conductance along its transient evolution, as shown in the inset of Figure 3f. This conductance change, however, is already considered in the determination of the statistics of α, which is obtained using all conductance readings during the experiments. In any case, these transients establish a lower dispersion limit which does not depend on sample-to-sample variations. However, this should not be a problem for the resistance standard because the conductance would saturate after few minutes. Notice that in the practical implementation of the resistance standard, the occurrence of the second event would play no role since the stress should finish after the generation of the first BD

© 2023 The Authors. Advanced Quantum Technologies published by Wiley-VCH GmbH

25119044, 2023, 7, Downloaded from https://onlinelibrary.wiley.com/doi/10.1002/qute.202300048 by Readcube (Labtiva Inc.), Wiley Online Library on [03/10/2023]. See the Terms and Conditions (https://onlinelibrary.wiley.com/terms-and-conditions) on Wiley Online Library for rules of use; OA articles are governed by the applicable Creative Commons License

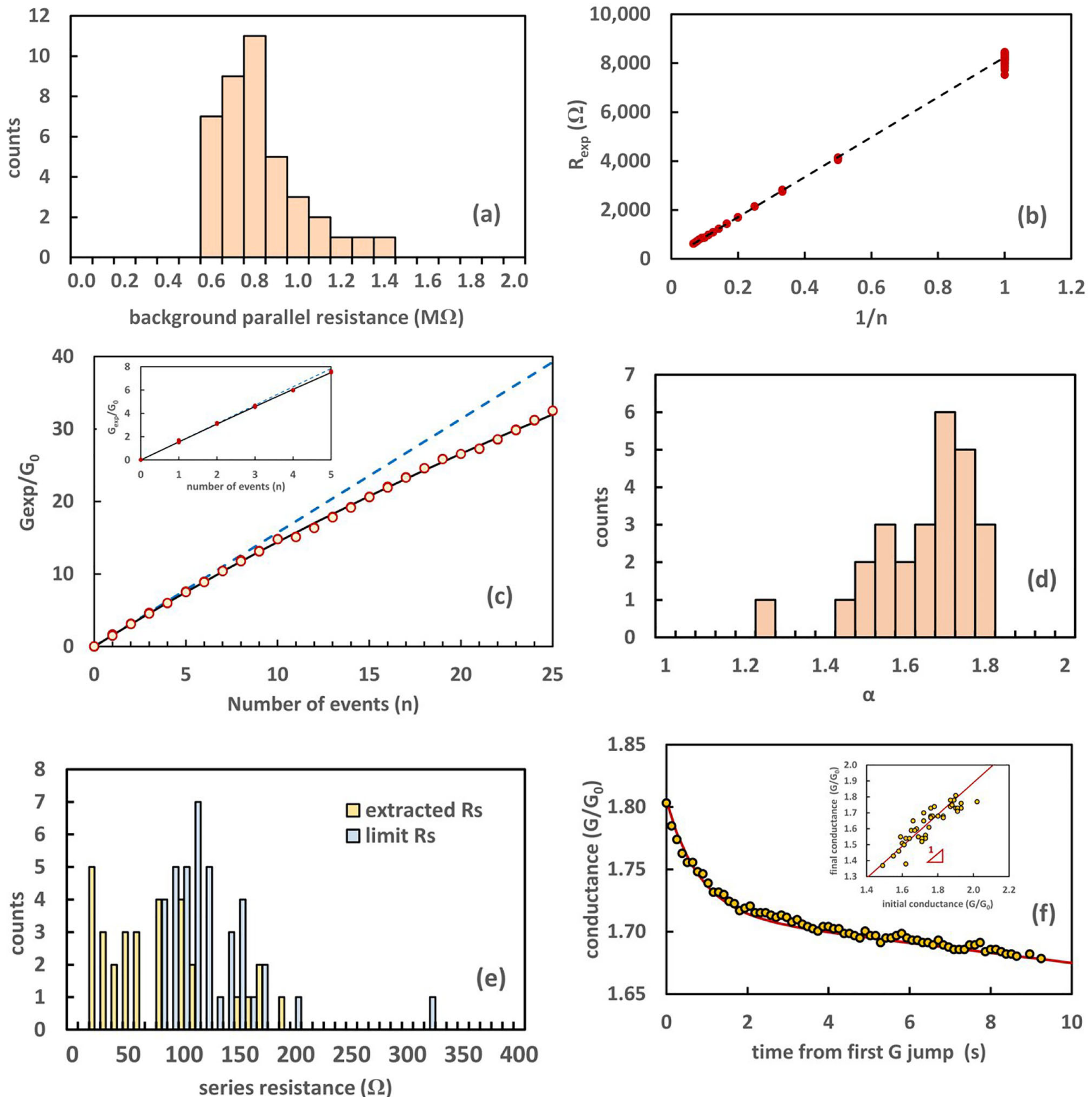

Figure 3. a) Histogram of the background resistance, R_B. b) Experimental resistance versus the inverse of the number of events for a single sample. Linear fit allows to extract α and R_S. c) Experimental conductance versus the number of events. Model (black line) is shown to fit the results (dots) and the dashed blue line corresponds to the ideal experimental conductance (i.e., without series resistance). The inset shows the detail for the first five events, showing that the impact of the series resistance is rather negligible for these events. d) Histogram of the extracted values of α for all the samples. e) Histogram of R_S for all samples, using the two methods explained in the text. f) Conductance transient after the first conductance jump in one sample. The red line is a fit of the data to Equation (5). The inset shows the correlation between initial and final conductance for the first BD event of all the samples (red line is a guide to the eye and has slope equal to one).

event and the reading of conductance would take place at a very low voltage, where no other BD event can be generated.

Further insight about the observed QPC phenomena can be obtained from the analysis of the statistics of current jumps between the conductance levels. Moreover, this can serve as a check of consistency for the proposed equivalent circuit model. Here, we consider the distribution of all the jumps ($n \approx 120$) in a single sample. The value of the conductance jumps as a function of the event number, n, is shown in **Figure 4**a. In an ideal device with $R_s = 0\ \Omega$, the jumps should be independent of n and equal to αG_0. However, the magnitude of the experimental jumps tends to decrease with n. If we account for the effect of R_s using

 © 2023 The Authors. Advanced Quantum Technologies published by Wiley-VCH GmbH

25119044, 2023, 7, Downloaded from https://onlinelibrary.wiley.com/doi/10.1002/qute.202300048 by Readcube (Labtiva Inc.), Wiley Online Library on [03/10/2023]. See the Terms and Conditions (https://onlinelibrary.wiley.com/terms-and-conditions) on Wiley Online Library for rules of use; OA articles are governed by the applicable Creative Commons License

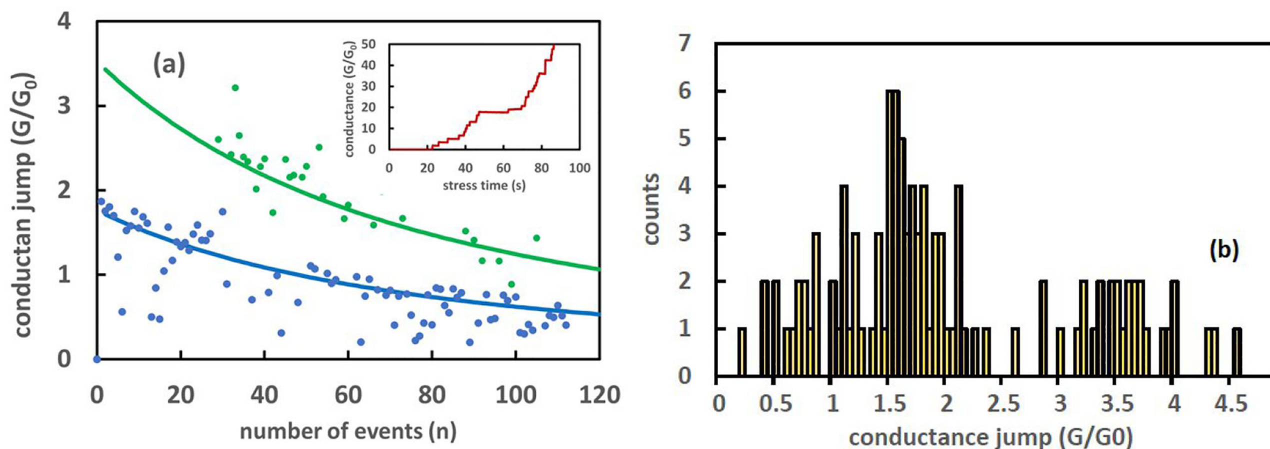

Figure 4. a) Magnitude of the measured conductance jumps as a function of n in one particular sample. Blue line corresponds to the constriction conductance jumps calculated from Equation (4), that is, taking the series resistance into account. Green line and dots correspond to experimental and theoretical double jumps, respectively. The inset shows the evolution of conductance during the stress that generates the jumps in the considered sample. b) Histogram of conductance jumps after correcting for the effect of the series resistance.

Equation (4), we see that the model nicely matches the experimental data (blue line in Figure 4a). It is also remarkable that there are larger conductance jumps (green points) which correspond to the creation of several CFs (or wider ones) at the same time. The green line corresponds to the model prediction for two concurrent jumps.

In Figure 4b, we report the histogram of conductance jumps after correcting the measured conductance for the effect of the series resistance. This correction is made by inverting Equation (4) to calculate $G_{\text{ideal}}(n) = G_{\text{exp}}(n)/[1 - R_s\, G_{\text{exp}}(n)]$ and the related jumps as $\Delta G_{\text{ideal}}\ (n \rightarrow n+1) = G_{\text{ideal}}\ (n+1) - G_{\text{ideal}}(n)$. As stated above, these jumps should ideally be equal to αG_0. However, the distribution shows two different peaks. One with an average conductance of $1.75G_0$ ($\alpha = 1.75$ in this sample) and the second centered around the double of this value, that is, $3.5G_0$. The width of these two peaks is wider than that of the distribution of α. This is because when considering the jumps, only one reading is considered for each event while all conductance points are considered for the statistics of the conductance levels. Thus, levels which are quite improbable from the point of view of the conductance distribution have the same weight in the distribution of jumps. The presence of the second peak indicates that, consistently with Figure 4a, in some cases two CFs (or a wider one) are formed within a very short time. This indicates that there are some propagation effects as previously reported in the literature.[45]

3. Discussion

In this section, we will discuss i) possible physics-based explanations for the measured conductance levels (i.e., the value of α and its variations) and ii) the implications of our results for the application of this type of QPC to a resistance standard.

Several physical phenomena can provide an explanation for the observed $1.67G_0$ conductance level, but all of them certainly involve several transmission modes because this conductance is larger than G_0. We have previously defined $\alpha \equiv gT$, where T is the transmission coefficient and g the number of 1D subbands contributing to conduction. Notice that, for simplicity, we have assumed that the transmission coefficient is the same for all the modes. T is the probability that an electron is transmitted from the left to right reservoir and vice versa, and it is related to backscattering from quasi-bound states arising from impurities, charge traps, non-adiabatic confining potential barrier, electron–electron interactions, etc. On the other hand, g can be related to different phenomena. In principle, if the transversal energy splitting is large enough, only those levels with minimum transversal energy (degenerate levels) will fall below the Fermi energy and contribute to the conduction. Notice that we have always assumed spin degeneracy ($g_s = 2$), which is implicit in considering G_0 as the quantization unit. Otherwise, conductance quantization should be given in terms of $G_0/2$ and the conductance levels should appear at half-integer multiples of G_0. Let us now consider the different factors that can influence the value of g. As stated above, in our samples, g must be larger than two but, as we will see, not necessarily equal to two.

First, we have to take into account that the Landauer transport model itself is a bit naïve at the atomic scale. In fact, both theoretical calculations and experimental results suggest that the measured conductance, at least for $G \geq G_0$, corresponds to the superposition of different eigenchannels associated to the valence atomic orbitals with transmission coefficient equal to or smaller than one.[48] Conductance measurements alone are not able to reveal the decomposition of conducting modes but other detailed experiments can deal with this subject, at least qualitatively.[48] What is undoubtful is that in the case $G \geq G_0$, the number of atomic channels must be larger than one. In previous publications, combined tight-binding calculations and experiments allowed to determine the number of eigenvalues contributing to the conduction in one-atom metal QPCs for a variety of materials.[50] However, since the transmission coefficient associated with these atomic orbitals is not necessarily 1, arbitrary values of α can be found.

Another aspect to consider is the fact the atomic-scale (geometrical) configuration of the CF bottleneck can determine the number of conducting modes, g. Since few atoms are involved

© 2023 The Authors. Advanced Quantum Technologies published by Wiley-VCH GmbH

25119044, 2023, 7, Downloaded from https://onlinelibrary.wiley.com/doi/10.1002/qute.202300048 by Readcube (Labtiva Inc.), Wiley Online Library on [03/10/2023]. See the Terms and Conditions (https://onlinelibrary.wiley.com/terms-and-conditions) on Wiley Online Library for rules of use; OA articles are governed by the applicable Creative Commons License

in the filament constriction, a change in their number or their spatial arrangement can give rise to changes in g. As mentioned above, Ohnishi et al. combined conductance measurements and HRTEM imaging to demonstrate that a single gold atom chain yields a conductance of G_0 while $2G_0$ was observed for a two-atom wide filament constriction.[7] Also emphasizing the role of the microscopic arrangement of atoms in the constriction, Krishnan used first-principles density functional theory (DFT) simulations to elucidate the impact of silver-based atomic-scale configurations on the conductance states of a QPC.[51] Their calculations and experiments showed that a two-atom chains are expected to exhibit $G = G_0$ while four and five-atom chains should exhibit conductance values slightly lower than $2G_0$. Their simulations showed that the transport modes are related to the structural/geometrical characteristics of a contact involving one or more atoms. Since in our experiments the formation of CFs is caused by electrical stress, the process is rather uncontrolled, and the structure of the filaments can be different from sample to sample and from event to event in a single device. This can certainly explain, not only the non-integer values of conductance peaks but also the rather large variations of conductance. The peak observed at $1.67G_0$ might correspond to a preferred atomic-scale configuration of the constriction. The observation of propagation effects (double jumps) might also correspond to the formation of a constriction involving more atoms at the very same location, that is, to a wider CF.

Another possible explanation for the observation of $G_{exp} \approx 2G_0$ is valley degeneracy. If the band structure has g_v minima in the longitudinal direction of transport one should expect conductance quantization in units of $g_v g_s G_0/2$ with g_v and g_s being the valley and spin degeneracies, respectively. This is a phenomenon that has been clearly observed in the case of split-gate induced semiconductor constrictions which are wide enough to keep the crystalline band structure.[52–54] Eventually, the most conclusive work about this issue is that of Bagraef, who evaluated the effect of the contributions of the different band valleys to conductance quantization in silicon nanowires defined by a three-gate structure but this has also been shown in other materials where values of g equal to $4e^2/h$ and $8e^2/h$ were reported.[35,36,48,52,55–59] In the case of our structures, we are dealing with "disordered" atomic-size constrictions without a clearly defined band structure so that the very concept of valley degeneracy might not apply. Thus, we do not expect that valley degeneracy is the reason for the observed $\approx 2G_0$ conductance unit in our experiments.

Another issue to consider is that the voltage drop can be asymmetric at both sides of the constriction.[60,61] Taking into account this injection asymmetry, it was demonstrated that the I–V characteristic of a QPC is given by

$$I = G_0 \left(\beta \overrightarrow{N} + (1 - \beta) \overleftarrow{N} \right) V \quad (6)$$

where $\overrightarrow{N}$ and $\overleftarrow{N}$ are the number of right- and left-going conduction modes, respectively.[61] This is a consequence of the specific energy location of the top of the confinement potential barrier at the QPC constriction with respect to the quasi-fermi levels at the reservoirs. For symmetrical potential drops at the two ends of the constriction ($\beta = 1/2$), Equation (6) reduces to $I = G_0 NV$, with $N = (\overrightarrow{N} + \overleftarrow{N})/2$, thus coinciding with the Landauer limit given by Equation (1). However, if $\overrightarrow{N}$ and $\overleftarrow{N}$ are even numbers (and still for $\beta = 1/2$) we find integer multiples of G_0 while for odd numbers of injecting channels, half-integer multiples of G_0 are predicted. These half-integer peaks have been widely reported, particularly in Valence Change Memory (VCM) devices, though they can also be explained by broken spin degeneracy, as previously discussed. In any case, when the applied voltage is large as in our stress experiments, the left-going modes are expected to be $\overleftarrow{N} = 0$ so that the conductance would be $G = \beta \overrightarrow{N} G_0$. According to this interpretation, depending on the value of β, different multiples of G_0 can be obtained. Notice that this could justify our results, $G \approx 1.67G_0$, if we assume $\overrightarrow{N} = 4$ and $\beta = 0.84$, in the absence of backscattering (i.e., for $T = 1$). Thus, in view of this analysis, a value of G_{exp} smaller than G_0 could also be attributed to the asymmetric distribution of the potential at the constriction/reservoir interfaces rather than to the reduction of the electron transmission related to backscattering.

Let us now consider the properties of oxygen vacancy paths, which are most likely the kind of CFs in our devices. As stated in the introduction, these paths are assumed to be responsible for filamentary resistive switching in VCM structures, and conductance quantization with integer and half-integer multiples of G_0 has been experimentally demonstrated in the literature. From first principles calculations, the transport properties of oxygen vacancy chains were studied in metal/monoclinic-HfO_2/metal and metal/amorphous-HfO_2/metal structures.[62] Using a Green's function formalism coupled with a DFT code, the conductance of filaments of different widths (varying number of atomic chains of vacancies in a single CF) was studied. It was shown that even the narrowest filaments (one-vacancy paths) can sustain conductive channels. For a one-vacancy chain, the conductance of crystalline HfO_2 was found to be $\approx G_0$ while in the amorphous material, the conductance levels are significantly lower than this value even for two and three-vacancies wide paths, thus suggesting that $T < 1$ is related to microscopic disorder. Since we are dealing with amorphous oxides, and considering that at least we have two conducting channels, this would eventually justify the observation of conductance values smaller than $2G_0$.

Another question which is relevant to our study is why conductance quantization is much better controlled in the nanolaminates than in the separate single-layer dielectrics. In this regard, it seems that combining layers with very important differences regarding the transport of oxygen ions allows to shape the CF and to control its electrical behavior. In particular, the fact that Al_2O_3 acts as a diffusion barrier might allow reducing the filament growth rate and hence favoring the creation of smaller (atomic size) filaments delivering reliable quantum transport properties.

As for the possible application of these QPCs for an on-chip resistance standard, we have to be able to trace back the measured resistance to the conductance quantum, which only depends on the fundamental constants, e and h. However, we have seen that there are non-idealities which affect the value of the measured conductance such as parasitic resistances (R_S, R_B, and R_P), asymmetric voltage drops at the QPC interfaces (β), and the transmission coefficient (T). If these values were constant in all the samples, we should be able to correct the measurements and

© 2023 The Authors. Advanced Quantum Technologies published by Wiley-VCH GmbH
25119044, 2023, 7, Downloaded from https://onlinelibrary.wiley.com/doi/10.1002/qute.202300048 by Readcube (Labtiva Inc.), Wiley Online Library on [03/10/2023]. See the Terms and Conditions (https://onlinelibrary.wiley.com/terms-and-conditions) on Wiley Online Library for rules of use; OA articles are governed by the applicable Creative Commons License

trace them back to G_0. The problem, however, is that all these parameters have inherent sample-to-sample variations that, in turn, cause variations in G_{exp}. In our samples, we have seen that the corrections related to R_S and R_B are significantly smaller ($\approx$ 2%) than those associated with the parameter α ($\approx$ 15%). The effects of T, β, and R_P are effectively considered within the value of α and it impossible to separate the individual contribution of these parameters to the total error. This is because all these parameters correspond to phenomena affecting the conductance of the CF itself, which is influenced by asymmetric voltage drops, backscattering, coupling of the quasi-1D modes to the reservoirs, and local series resistances. Using a circuit terminology, we can say that this is like having circuit elements connected in series in which the internal nodes are inaccessible. Ultimately, the device-to-device variability of conductance is related to the intrinsic stochasticity of atomic rearrangements during the formation of the CFs and this is likely the most difficult challenge to build up a reliable conductance standard.

Compared to other systems, to our knowledge, the best results regarding the control of quantized conductance in RS devices are those reported by the group of Hwang.[30] They reported up to 64 separate conductance levels considering cycle-to-cycle variations. However, they acknowledged that device-to-device variations due to changes in the number of atoms in the QPC constrictions are an important challenge. In this regard our results for single devices are similar regarding the control of the CF properties. In particular, we have demonstrated the creation of more than 60 BD filaments (in single devices) with non-overlapping conductance peaks and a conductance dispersion of less than $0.1G_0$ (Figure 2b) in spite of the conductance transients previously reported in Figure 3f. Thus, from a resistance standard point of view, our results for a single device are comparable to those of Hwang.[30] As far as device-to-device variations are concerned, a fair comparison is not possible since they did not report any results.

Another important requirement for the resistance standard application is to have sufficient filament stability to measure the conductance for the calibration processes. In the case of using RS devices, the filament would be reformed (SET) before each conductance measurement. Since measurement takes a short time, only a limited retention of the low resistance state is required, contrary to what happens for nonvolatile memory or neuromorphic applications. In the case of using BD paths (as considered in this paper), retention is indeed an important figure of merit since the CF should always keep the same value of conductance during the whole life of the circuit. In this regard, it is important to remark that in our experiments we have not found any reverse event even when applying a voltage of opposite polarity. This means that we are indeed dealing with irreversible filaments that are one-time programmable. Although we have not evaluated low-voltage retention explicitly, no other BD event is expected to occur if we create the first CF at a high voltage and then measure the conductance (every time that is needed for calibration) at a much lower voltage (the read voltage). Notice that the breakdown field is of the order of 8 MV cm^{-1} as shown in Figure 1a. A systematic study of the evolution of conductance at low voltage is certainly required (conductance drift, fluctuations, random telegraph noise, etc.). However, as far as the occurrence of subsequent BD events we must remark that the voltage acceleration of BD is known to be highly non-linear. Using CVS at different voltages, we have demonstrated that the well-known E-model for voltage acceleration nicely fits the BD data for the nanolaminate samples.[47] This model states that the voltage dependence of the characteristic time to BD (T_{BD}) is given by $T_{BD} = T_{BD0}\exp(-\gamma V)$. For our samples, we have determined that the voltage acceleration factor is $\gamma = 4.8$ V^{-1} and hence, given that $T_{BD} \approx 35$ s at -7 V, the time to breakdown at a read voltage of 0.2 V would be $\approx 10^{15}$s. Of course, this is a rough extrapolation, but it provides unquestionable evidence that the first conductance level is not expected to be disrupted by another BD event at low measuring voltages.

Another possible issue for the resistance standard application are propagation effects. Indeed, we have observed that higher-order BD events are prone to show propagation effects (double jumps). Although in our measurements these effects have not been observed for the first filament formation, they cannot be discarded because the considered statistical sample size is relatively small. Further study of the stability and control of the first BD event is certainly required.

In any case, having a fixed value of conductance (not depending on RS cycle-to cycle variations) would be a great advantage of using BD filaments (instead of RS devices) for an on-chip resistance standard, provided that sample to sample variations could be controlled by an appropriate choice of the insulator and the electroforming process.

4. Conclusions

We have presented clear evidence of quantized conductance levels in QPCs created by irreversible BD events in nanolaminate Al_2O_3/HfO_2 structures. We have suggested to use these effects for the novel application of an on-chip resistance standard. Among the application requirements, we have focused on stochasticity (due to atomic-scale variations of the CF in different devices) and on the impact of parasitic resistances. Since this application only requires one conductance level, we have focused on the first one, which is centered at $G_{exp} \approx 1.67\ G_0$. We have discussed different phenomena which can give rise to conductance peaks at non-integer multiples of G_0, and we have stated that at least two conducting modes are required to explain our results. We have concluded that the most likely reasons why the measured conductance is smaller than $2G_0$ are backscattering ($T < 1$), and/or asymmetric voltage drops ($\beta \neq 0.5$) at the QPC/reservoir interfaces. Moreover, we have discussed the role of the local access series resistance to the QPC constriction.

On the basis of the previous results, we have proposed to apply conductance quantization in irreversible BD filaments for the implementation of an on-chip resistance standard. At this point, however, sample-to-sample variations ($\approx$15%) are still too large for this application. Notice that the accuracy of off-the-shelf resistances can be as high as 0.01% and that the quantum Hall resistance standard has an uncertainty of only $\approx 10^{-9}$.[59] Nevertheless, although our results are yet far from the required accuracy, they are comparable to (or better than) those obtained with any resistive switching device so far. Appropriate control by insulator design and electrical stress methods are expected to allow a better control of the shape of the filament and hence reduce the

© 2023 The Authors. Advanced Quantum Technologies published by Wiley-VCH GmbH

25119044, 2023, 7, Downloaded from https://onlinelibrary.wiley.com/doi/10.1002/qute.202300048 by Readcube (Labtiva Inc.), Wiley Online Library on [03/10/2023]. See the Terms and Conditions (https://onlinelibrary.wiley.com/terms-and-conditions) on Wiley Online Library for rules of use; OA articles are governed by the applicable Creative Commons License

sample-to-sample variations as required for the resistance standard application.

In conclusion, from the results presented in this paper, it follows that it is worthwhile exploring the possible implementation of an on-chip resistance standard based on oxide BD events showing QPC effects.[21]

5. Experimental Section

Device Fabrication: Three types of dielectric layers were deposited by atomic-layer deposition on a p^+-Si (100) wafer with resistivity of 0.1–1.4 Ω cm. HfO_2 and Al_2O_3 single layers of ≈ 10 nm and a 5-layer nanolaminate stack ($Al_2O_3/HfO_2/Al_2O_3/HfO_2/Al_2O_3$) of roughly the same total thickness (≈2 nm each layer). Note that in all cases an ultrathin layer was expected to be formed at the Si interface, the so-called native oxide. Al electrodes were deposited on top of the insulator and to contact the back of the Si wafer to form large-area (6.4×10^3, 1.44×10^3, 3.24×10^4, and 9.6×10^5 μm^2) devices. Full details of the fabrication process can be found in a previous publication.[26] Although the as-deposited nanolaminate layers show well-defined and sharp interfaces for each film, as shown by high-resolution electron microscopy, if a high-temperature post-deposition annealing is performed, this ordered structure vanishes. The resulting "mixed" dielectric had intermediate properties with respect to those of the constituting materials. In this work, the interest was related to engineering the shape of BD conducting filaments in the atomic-size limit and to this goal, an ordered structure of the nanolaminate is needed. Thus, all the presented results corresponded to the as-deposited dielectrics, that is, without any post-deposition treatment.

Measurements: All electrical measurements were performed with an Agilent 4156C Semiconductor Parameter Analyzer. The bottom contact was grounded, and a negative voltage was applied to the gate contact to ensure injection from the top electrode. Injection from the substrate would require inverting the substrate (Si wafer is p-type). For these measurements, the largest area samples (9.6×10^5 μm^2) which facilitate the observation of successive BD events in a reasonable time under the application of relatively small gate voltages were chosen.

Acknowledgements

E.M. and J.S. acknowledge the support provided by the European project MEMQuD, code 20FUN06, which has received funding from the EMPIR program cofinanced by the Participating States and from the European Union's Horizon 2020 research and innovation program. F.A. acknowledges financial support from MICINN (Spain) through the programme Juan de la Cierva-Formación grant number FJC2021-046808-I. IMB authors thank CSIC funding through project 20225AT012. M.B.G. acknowledges the Ramón y Cajal grant number RYC2020-030150-I.

Conflict of Interest

The authors declare no conflict of interest.

Data Availability Statement

The authors agree to share relevant data upon justified demand.

Keywords

conductance quantization, dielectric breakdown, metrology, resistance standard

Received: February 28, 2023
Revised: April 11, 2023
Published online: May 18, 2023

[1] R. Landauer, *IBM J. Res. Dev.* **1957**, *16*, 223.
[2] S. Datta, *Electronic Transport in Mesoscopic Systems*, Cambridge University Press, Cambridge **1997**.
[3] B. J. Van Wees, H. Van Houten, C. W. J. Beenakker, J. G. Williamson, L. P. Kouwenhoven, D. Van Der Marel, C. T. Foxon, *Phys. Rev. Lett.* **1988**, *60*, 848.
[4] D. A. Wharam, T. J. Thornton, R. Newbury, M. Pepper, H. Ahmed, J. E. F. Frost, D. G. Hasko, D. C. Peacock, D. A. Ritchie, G. A. C. Jones, *J. Phys. C: Solid State Phys.* **1988**, *21*, L209.
[5] J. M. Krans, J. M. van Ruitenbeek, V. V. Fisun, I. K. Yanson, L. J. de Jongh, *Nature* **1995**, *375*, 767.
[6] J. I. Pascual, J. Mendez, J. Gomez-Herrero, A. M. Baro, N. Garcia, U. Landman, W. D. Luedtke, E. N. Bogachek, H. P. Cheng, *Science* **1995**, *267*, 1793.
[7] H. Ohnishi, Y. Kondo, K. Takayanagi, *Nature* **1988**, *395*, 780.
[8] C. Z. Li, A. Bogozi, W. Huang, N. J. Tao, *Nanotechnology* **1999**, *10*, 221.
[9] J. Suñé, E. Miranda, in *Int. Electron Devices Meeting Technical Digest*, IEEE, New York **2000**, p. 533.
[10] S. Tappertzhofen, I. Valov, R. Waser, *Nanotechnology* **2012**, *23*, 145703.
[11] T. Tsuruoka, T. Hasegawa, K. Terabe, M. Aono, *Nanotechnology* **2012**, *23*, 435705.
[12] S. Long, X. Lian, C. Cagli, X. Cartoixà, R. Rurali, E. Miranda, D. Jiménez, L. Perniola, M. Liu, J. Suñé, *Appl. Phys. Lett.* **2013**, *102*, 183505.
[13] J. J. T. Wagenaar, M. Morales-Masis, J. M. van Ruitenbeek, *J. Appl. Phys.* **2012**, *111*, 014302.
[14] K. Terabe, T. Hasegawa, T. Nakayama, M. Aono, *Nature* **2005**, *433*, 47.
[15] W. Xue, S. Gao, J. Shang, X. Yi, G. Liu, R. W. Li, *Adv. Electron. Mater.* **2019**, *5*, 1800854.
[16] G. Milano, M. Aono, L. Boarino, U. Celano, T. Hasegawa, M. Kozicki, S. Majumdar, M. Menghini, E. Miranda, C. Ricciardi, S. Tappertzhofen, K. Terabe, I. Valov, *Adv. Mater.* **2022**, *34*, 2201248.
[17] X. Lian, X. Cartoixa, E. Miranda, L. Perniola, R. Rurali, S. Long, M. Liu, J. Suñé, *J. Appl. Phys.* **2014**, *115*, 244507.
[18] E. Miranda, J. Suñé, in *39th Annual Int. Reliability Physics Symp. Proceedings*, IEEE, New York **2001**, p. 367.
[19] R. Degraeve, P. Roussel, L. Goux, D. Wouters, J. Kittl, L. Altimime, M. Jurczak, G. Groeseneken, in *Int. Electron Devices Meeting Technical Digest*, IEEE, New York **2010**, p. 28.4.1.
[20] J. van Ruitenbeek, M. Morales Masis, E. Miranda, in *Resistive Switching: From Fundamentals of Nanoionic Redox Processes to Memristive Device Applications* (Eds: D. Ielmini, R. Waser), Wiley-VCH, Weinheim **2016**, p. 197.
[21] G. Milano, F. Ferrarese-Lupi, M. Fretto, C. Ricciardi, N. De Leo, L. Boarino, *Adv. Quantum Technol.* **2020**, *3*, 2000009.
[22] M. H. Cho, Y. S. Roh, C. N. Whang, K. Jeong, H. J. Choi, S. W. Nam, D. H. Ko, J. H. Lee, N. I. Lee, K. Fujihara, *Appl. Phys. Lett.* **2002**, *81*, 1071.
[23] R. Lo Nigro, E. Schilirò, P. Fiorenza, F. Roccaforte, *J. Vac. Sci. Technol., A* **2020**, *38*, 032410.
[24] S. J. Ding, H. Hu, C. Zhu, S. J. Kim, X. Yu, M. F. Li, B. J. Cho, D. S. H. Chan, M. B. Yu, S. C. Rustagi, A. Chin, D. L. Kwong, *IEEE Trans. Electron Devices* **2004**, *51*, 886.
[25] A. Kartci, S. Vancik, J. Prasek, R. Hrdy, M. Schneider, U. Schmid, J. Hubalek, *Mater. Today Commun.* **2022**, *33*, 104664.

© 2023 The Authors. Advanced Quantum Technologies published by Wiley-VCH GmbH

25119044, 2023, 7, Downloaded from https://onlinelibrary.wiley.com/doi/10.1002/qute.202300048 by Readcube (Labtiva Inc.), Wiley Online Library on [03/10/2023]. See the Terms and Conditions (https://onlinelibrary.wiley.com/terms-and-conditions) on Wiley Online Library for rules of use; OA articles are governed by the applicable Creative Commons License

[26] F. Campabadal, J. M. Raf, M. Zabala, O. Beldarrain, A. Faigón, H. Castán, A. Gómez, H. García, S. Dueñas, *J. Vac. Sci. Technol., B: Nanotechnol. Microelectron.: Mater., Process., Meas., Phenom.* **2011**, *29*, 01AA07.
[27] R. Nakamura, T. Toda, S. Tsukui, M. Tane, M. Ishimaru, T. Suzuki, H. Nakajima, *J. Appl. Phys.* **2014**, *116*, 033504.
[28] S. Zafar, H. Jagannatha, L. F. Edge, D. Gupta, *Appl. Phys. Lett.* **2011**, *98*, 152903.
[29] F. Aga, J. Woo, Hyunsang Hwang, *Nanotechnology* **2017**, *28*, 115707.
[30] W. Banerjee, H. Hwang, *Adv. Electron. Mater.* **2019**, *5*, 1900744.
[31] C. Mahata, M. Ismail, S. Kim, *Appl. Phys. Lett.* **2021**, *119*, 221601.
[32] W. Xue, Y. Li, G. Liu, Z. Wang, W. Xiao, K. Jiang, Z. Zhong, S. Gao, J. Ding, X. Miao, X. H. Xu, R. W. Li, *Adv. Electron. Mater.* **2020**, *6*, 1901055.
[33] S. Lim, C. Sung, H. Kim, T. Kim, J. Song, J. J. Kim, H. Hwang, *IEEE Electron Device Lett.* **2018**, *39*, 312.
[34] A. Gómez, H. Castán, H. García, S. Dueñas, L. Bailón, F. Campadal, J. sM. Rafí, M. Zabala, *J. Vac. Sci. Technol., B* **2011**, *29*, 01A901.
[35] A. Conde, C. Martínez, D. Jiménez, E. Miranda, J. M. Rafí, F. Campabadal, J. Suñé, *Solid-State Electron.* **2012**, *71*, 48.
[36] J. Suñé, S. Tous, E. Y. Wu, *IEEE Electron Device Lett.* **2009**, *30*, 1359.
[37] J. Suñé, *IEEE Electron Device Lett.* **2001**, *22*, 296.
[38] J. H. Stathis, *J. Appl. Phys.* **1999**, *86*, 5757.
[39] J. Muñoz-Górriz, M. B. González, F. Campabadal, J. Suñé, E. Miranda, *Microelectron. Reliab.* **2020**, *114*, 113748.
[40] J. Muñoz-Górriz, M. B. González, F. Campabadal, J. Suñé, E. Miranda, *IEEE Electron Device Lett.* **2020**, *41*, 1770.
[41] E. Y. Wu, B. Li, J. H. Stathis, *Appl. Phys. Lett.* **2013**, *103*, 152907.
[42] E. Y. Wu, B. Li, J. H. Stathis, R. Achanta, in *Int. Electron Devices Meeting Technical Digest*, IEEE, New York **2014**, p. 480.
[43] A. Alam, K. Smith, in *41st Annual Int. Reliability Physics Symp. Proceedings* IEEE, New York **2003**, p. 406.
[44] J. Suñé, E. Y. Wu, W. L. Lai, *IEEE Trans. Electron Devices* **2004**, *51*, 1584.
[45] S. Lombardo, F. Crupi, A. La Magna, C. Spinella, A. Terrasi, A. LaMantia, B. Neri, *J. Appl. Phys.* **1998**, *84*, 472.
[46] C. H. Tung, K. L. Pey, W. H. Lin, M. K. Radhakrishnan, *IEEE Electron Device Lett.* **2002**, *23*, 526.
[47] J. W. McPherson, *Microelectron. Reliab.* **2012**, *52*, 1753.
[48] N. Agraït, A. Levy Yeyati, J. M. vanRuitenbeek, *Phys. Rep.* **2003**, *377*, 81.
[49] S. Gao, C. Chen, Z. Zhai, H. Y. Liu, Y. S. Lin, S. Z. Li, S. H. Lu, G. Y. Wang, C. Song, F. Zeng, F. Pan, *Appl. Phys. Lett.* **2014**, *105*, 063504.
[50] E. Scheer, N. Agraït, J. C. Cuevas, A. L. Yeyati, B. Ludoph, A. Martín-Rodero, G. Rubio-Bollinger, J. M. van Ruitenbeek, C. Urbina, *Nature* **1998**, *394*, 154.
[51] K. Krishnan, M. Muruganathan, T. Tsuruoka, H. Mizuta, M. Aono, *Jpn. J. Appl. Phys.* **2017**, *56*, 06GF02.
[52] D. Tobben, D. A Wharam, G. Abstreiter, J. P. Kolthaus, F. Schaffler, *Semicond. Sci. Technol.* **1995**, *10*, 711.
[53] O. Gunawan, B. Habib, E. P. De Poortere, M. Shayegan, *Phys. Rev. B* **2006**, *74*, 155436.
[54] S. Goswami, K. A. Slinker, M. Friesen, L. M. McGuire, J. L. Truitt, C. Tahan, L. J. Klein, J. O. Chu, P. M. Mooney, D. W. van der Weide, R. Joynt, S. N. Coppersmith, M. A. Eriksson, *Nat. Phys.* **2007**, *3*, 41.
[55] N. T. Bagraev, A. D. Buravlev, L. E. Klyachkin, A. M. Malyarenko, W. Gehlhoff, V. K. Ivanov, I. A. Shelykh, *Semiconductors* **2002**, *36*, 439.
[56] K. Sakanashi, N. Wada, K. Murase, K. Oto, G. H. Kim, K. Watanabe, T. Taniguchi, J. P. Bird, D. K. Ferry, N. Aoki, *Appl. Phys. Lett.* **2021**, *118*, 263102.
[57] H. Overweg, H. Eggimann, X. Chen, S. Slizovskiy, M. Eich, R. Pisoni, Y. Lee, P. Rickhaus, K. Watanabe, T. Taniguchi, V. Fal'ko, T. Ihn, K. E. Mcpherson, *Nano Lett.* **2018**, *18*, 553.
[58] G. Scappucci, L. Di Gaspare, E. Giovine, A. Notargiacomo, R. Leoni, F. Evangelisti, *Phys. Rev. B* **2006**, *74*, 03532.
[59] R. Ribeiro-Palau, F. Lafont, J. Brun-Picard, D. Kazazis, A. Michon, F. Cheynis, O. Couturaud, C. Consejo, B. Jouault, W. Poirier, F. Schopfer, *Nat. Nanotechnol.* **2015**, *10*, 965.
[60] L. P. Kouwenhoven, B. J. van Wees, C. J. P. M. Harmans, J. G. Williamson, H. van Houten, C. W. J. Beenakker, C. T. Foxon, J. J. Harris, *Phys. Rev. B* **1989**, *39*, 8040.
[61] E. Miranda, S. Kano, C. Dou, K. Kakushima, J. Suñé, H. Iwai, *Appl. Phys. Lett.* **2012**, *101*, 012910.
[62] X. Cartoixà, R. Rurali, J. Suñé, *Phys. Rev. B* **2012**, *86*, 165445.

© 2023 The Authors. Advanced Quantum Technologies published by Wiley-VCH GmbH

25119044, 2023, 7, Downloaded from https://onlinelibrary.wiley.com/doi/10.1002/qute.202300048 by Readcube (Labtiva Inc.), Wiley Online Library on [03/10/2023]. See the Terms and Conditions (https://onlinelibrary.wiley.com/terms-and-conditions) on Wiley Online Library for rules of use; OA articles are governed by the applicable Creative Commons License